Broadband Unidirectional Scattering by Magneto-Electric Core–Shell Nanoparticles

Wei Liu, Andrey E. Miroshnichenko, Dragomir N. Neshev, and Yuri S. Kivshar*

Nonlinear Physics Centre, Centre for Ultrahigh-Bandwidth Devices for Optical Systems (CUDOS), Research School of Physics and Engineering, Australian National University, Canberra, ACT 0200, Australia

ABSTRACT Core–shell nanoparticles have attracted surging interests due to their flexibly tunable resonances and various applications in medical diagnostics, biosensing, nanolasers, and many other fields. The core–shell nanoparticles can support simultaneously both electric and magnetic resonances, and when the resonances are properly engineered, entirely new properties can be achieved. Here we study core–shell nanoparticles that support both electric and artificial magnetic dipolar modes, which are engineered to coincide spectrally with the same strength. We reveal that the interferences of these two resonances result in azimuthally symmetric unidirectional scattering, which can be further improved by arranging the nanoparticles in a chain, with both azimuthal symmetry and vanishing backward scattering preserved over a wide spectral range. We also demonstrate that the vanishing backward scattering is preserved, even for random particle distributions, which can find applications in the fields of nanoantennas, photovoltaic devices, and nanoscale lasers that require backward scattering suppressions.

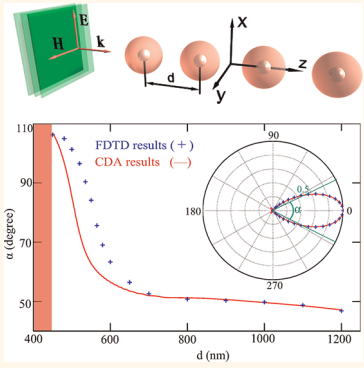

KEYWORDS: Mie scattering · core–shell nanoparticle · dielectric magnetic response · coupling of electric and magnetic dipoles · broadband unidirectional scattering

The study of light scattering by small particles has a long history and is of fundamental significance in different branches of physics, such as sensing, solar cells, optical communications, *etc*. Nanoparticles have found wide applications for biomedical labeling, impacting strongly on fields such as biology and medical research.[1−5] Recently fostered by the flourishing fields of plasmonics and metamaterials, various novel scattering phenomena have been demonstrated, for example, cloaking,[6] superscattering,[7,8] control of the direction of the scattered light,[9,10] nonlinear second harmonic scattering,[11] and artificial antiferromagnetism.[12] It is also shown that light scattering can be significantly enhanced with the incorporation of gain materials, based on which deep subwavelength nanoscale lasing could be achieved.[13−15]

For many applications based on the mechanism of resonant light scattering, such as nanoantennas,[16,17] sensing with nanoparticles,[18] and photovoltaic devices,[4] usually broadband unidirectional scattering is required or preferred. However, for light scattering by particles at resonant wavelengths, usually only one specific mode is dominantly excited. Consequently, two typical features of the scattering patterns are exhibited: (i) light will be scattered symmetrically in backward and forward directions,[1] and (ii) the excited mode will have a different orientation depending on the polarization of the incident wave, resulting in azimuthally asymmetric scattering patterns.[1,19] To suppress the unwanted backward scattering (reflection) and enhance the directional forward scattering, an extra reflector or coupled item,[16,17,20−24] an extended substrate,[24−27] Fabry-Pérot resonator-like structures,[26,28] and/or complicated structure engineering[29,30] are usually employed. It was theoretically predicted that a magnetic particle can exhibit unidirectional scattering[31−33] without involving complicated structures or an extra reflector. However, the high loss and limited operating wavelengths of magnetic materials can prevent the broadband unidirectional scattering and hinder possible practical applications. Although it is shown that the backward scattering suppression can be achieved in a single high permittivity sphere,[34,35] or in simple structures with anisotropic materials,[36,37] the operating spectral regime is far from the resonant region and the scattering is generally weak in all directions,[34,35] without significant forward scattering enhancement.

* Address correspondence to ysk124@physics.anu.edu.au.

Received for review March 30, 2012 and accepted April 30, 2012.

Published online April 30, 2012
10.1021/nn301398a

In this paper, we demonstrate the suppression of the backward scattering and enhancement of the forward directional scattering by superimposing electric and artificial magnetic dipolar responses of core−shell nanoparticles. We achieve azimuthally symmetric broadband unidirectional scattering using the (metal) core−(dielectric) shell nanoparticle structures without magnetic materials or extra reflectors being involved. Each nanoparticle is effectively magneto-electric as it supports orthogonal electric dipole (ED) and artificial magnetic dipole (MD) resonances, which can be engineered to coincide spectrally with the same strength.[38,39] The electric and magnetic dipoles have the same strength, and they can interfere destructively in the backward direction and constructively in the forward direction. Therefore, azimuthally symmetric unidirectional scattering can be achieved even for a single particle. Furthermore, we show that the directionality can be additionally enhanced in a chain of such particles. Although there is a trade-off between energy confinement and directionality for different interparticle distances, the properties of vanishing backward scattering and azimuthal symmetry are always preserved. At the end, we demonstrate that the operating spectral regime of the unidirectional scattering is broadband and the feature of vanishing backward scattering is preserved, even for a random ensemble of such magneto-electric core−shell particles.

RESULTS AND DISCUSSION

The scattering of a spherical particle (see Figure 1a) (single-layered or multilayered) can be solved analytically using Mie theory.[1,40] The effective electric and magnetic dipolar polarizabilities can be expressed as[1]

$$\alpha_1^e = \frac{3i}{2k^3}a_1,\ \alpha_1^m = \frac{3i}{2k^3}b_1 \qquad (1)$$

where a_1 and b_1 are Mie scattering coefficients, which correspond to electric and magnetic dipole moments, respectively, and k is the angular wavenumber in the background material (vacuum in our case). In Figure 1b, we show the scattering efficiency spectra including the total scattering − total scattering cross section divided by the geometrical cross section of the particle (blue line) and the scattering contribution from a_1 (red line) of a silver sphere with a radius R = 68 nm, illuminated by a linearly polarized (along x) plane wave, as shown in Figure 1a. For the permittivity of silver, we use the experimental data from ref 41. It is clear that the sphere can be approximated as an electric dipole for the wavelength range under consideration. The scattering patterns at the resonant wavelength of 440 nm are shown on the right of Figure 1c for both p (line with crosses) and s (solid line) polarizations [scattering plane parallel (φ = 0) and perpendicular to the polarization (φ = 90°) of the incident plane wave, respectively]. The three-dimensional (3D) scattering pattern is shown on the left of Figure 1c with a part cut off for better visibility. Two typical features of the scattering by a single dipole are seen: (i) azimuthal asymmetry and (ii) symmetry in the backward and forward directions. We note that the spherical symmetry of the silver sphere does not guarantee azimuthally symmetric scattering because the sphere has only dominant electric response.

In contrast, in Figure 1d, we show the scattering efficiency spectra for a core−shell nanoparticle (total and the contribution from a_1 and b_1) with a silver core and dielectric shell of refractive index n = 3.4 (*e.g.*, GaAs, Si, or Ge) with an inner radius R_1 = 68 nm and an outer radius R_2 = 225 nm (inset). Considering that a_1 and b_1 correspond to the first-order electric and magnetic eigenmodes of the core−shell nanoparticle, respectively, the core−shell nanoparticle can be effectively viewed as a combination of a pair of orthogonal electric and magnetic dipoles. We note here that spherical symmetry leads to the orthogonality of the two modes, and thus they are not coupled to each other.[42] Due to the orthogonality, it is possible to superimpose these two modes spectrally. To match the strength of the electric and magnetic dipoles with the same strength, further geometric tuning (change of the radius aspect ratios) is required.[38,39] For most structures that do not exhibit specific symmetries,[42] although both electric and magnetic resonances are supported, they are coupled to each other and therefore the resonances are spectrally separated. Due to the coexistence of ED and MD resonances, different from a single metal sphere, the core−shell nanoparticle is effectively a magneto-electric scatterer according to eq 1.

When higher order mode excitation is negligible ($a_n = b_n = 0, n \geq 2$), the normalized scattering intensity (NSI, which corresponds to the scattering intensity normalized by the intensity of the incident wave[1]) of a spherical particle can be derived as

$$\mathrm{NSI}(\theta,\varphi) = \frac{9}{4k^2}[\sin^2\varphi(a_1+b_1\cos\theta)^2 + \cos^2\varphi(a_1\cos\theta+b_1)^2] \qquad (2)$$

When there is no dipolar magnetic response ($b_1 = 0$), as for the case of a silver sphere in Figure 1b, the scattering intensity is $\mathrm{NSI}(\theta,\varphi) = (9/4k^2)a_1^2(\sin^2\varphi + \cos^2\varphi\cos\theta^2)$, which results in a typical scattering pattern of an electric dipole, as shown in Figure 1c. However, when there are equal dipolar electric and magnetic responses ($b_1 = a_1 = c$), as for the core−shell nanoparticle shown in Figure 1d, the scattering intensity is simplified to

$$\mathrm{NSI}(\theta) = \frac{9}{4k^2}c^2(1+\cos\theta)^2 \qquad (3)$$

where the φ dependence is eliminated, indicating that the scattering is azimuthally symmetric, as

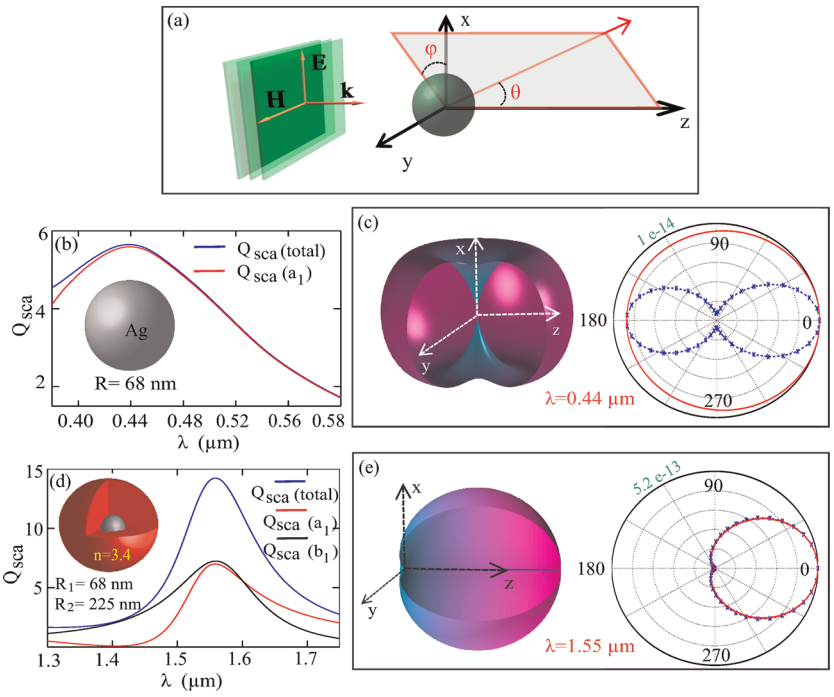

Figure 1. Scattering of an incident plane wave by a spherical particle. The electric field is polarized along *x*, and the wave is propagating along *z*. (b) Scattering efficiency spectra (total and the contribution from a_1) for a Ag sphere (inset) with a radius of 68 nm. (c) Left: corresponding 3D scattering pattern at the resonant wavelength of 440 nm (with a part cut for bettering viewing). Right: scattering pattern for both s (solid line) and p (line with crosses) polarizations. (d) Scattering efficiency spectra (total and the contributions from a_1 and b_1) for a core−shell nanoparticle (inset) with an inner radius of 68 nm and an outer radius of 225 nm. The core is silver, and shell is dielectric with n = 3.4. (e) Left: corresponding 3D scattering pattern at the resonant wavelength of 1550 nm. Right: scattering patterns for both p and s polarizations. In (c) and (e), the maximum normalized scattering intensity is shown in green on the side, as is the case for other figures below.

shown in Figure 1e. Also according to eq 3, the forward scattering intensity is NSI(0) = $9c^2/k^2$, which is enhanced, and the backward normalized scattering intensity is NSI(π) = 0, which is canceled. The enhancement and cancelation of the scattering originates from constructive and destructive interference of the electric and magnetic dipoles, respectively.

Up to now, we have demonstrated azimuthally symmetric unidirectional scattering using a single core−shell nanoparticle (eq 3 and Figure 1e). To further enhance the directionality, we employ a one-dimensional chain of such particles with a chain axis parallel to the propagation direction of the incident plane wave (Figure 2a), where the interparticle distance is d. To characterize the directionality of the scattering, we define the main lobe angular beamwidth α, as shown in Figure 2b, which corresponds to the full width at half-maximum of the scattering intensity. To investigate theoretically the scattering of the chain, each core−shell nanoparticle is treated as a combination of orthogonal ED and MD with polarizabilities described by eq 1. The chain comprises N such particles, and the ith particle, located at the position of r_i, has an electric moment d_i and a magnetic moment m_i. According to the coupled dipole approximation (CDA) involving both electric and magnetic dipoles[43,44]

$$\begin{aligned} d_i &= \alpha_1^e E_i^0 + \alpha_1^e \sum_{j=1:N}^{j\neq i} (E_i^{d_j} + E_i^{m_j}) \\ m_i &= \alpha_1^m H_i^0 + \alpha_1^m \sum_{j=1:N}^{j\neq i} (H_i^{d_j} + H_i^{m_j}) \end{aligned} \quad (4)$$

where E_i^0 and H_i^0 are the electric and magnetic fields of the incident wave at position r_i, respectively; $E_i^{d_j}$ and $H_i^{d_j}$ are electric and magnetic fields of radiation of d_j at r_i, respectively; $E_i^{m_j}$ and $H_i^{m_j}$ are the fields of radiation of m_j at r_i. By solving eq 4, both the electric and magnetic moments of each particle can be obtained and then the scattering pattern can be found as the superposition of the radiations of all the 2N interacting dipolar moments.

The symmetry of Maxwell's equations guarantees that in eq 4 d_i and $-m_i$, E_i and $-H_i$ are exchangeable when $\alpha_1^e = \alpha_1^m$. This means that each particle in the chain will have electric and magnetic moments of the same strength, thus leading to unidirectional scattering, similar to an isolated core−shell nanoparticle. Considering also the azimuthal symmetry of the structure, the whole chain will scatter light unidirectionally independent of the azimuthal angle. In Figure 2b−d, we show the scattering patterns at arbitrary scattering planes by a chain with particle number N = 2, 3, and 10, according to eq 4. The operating wavelength

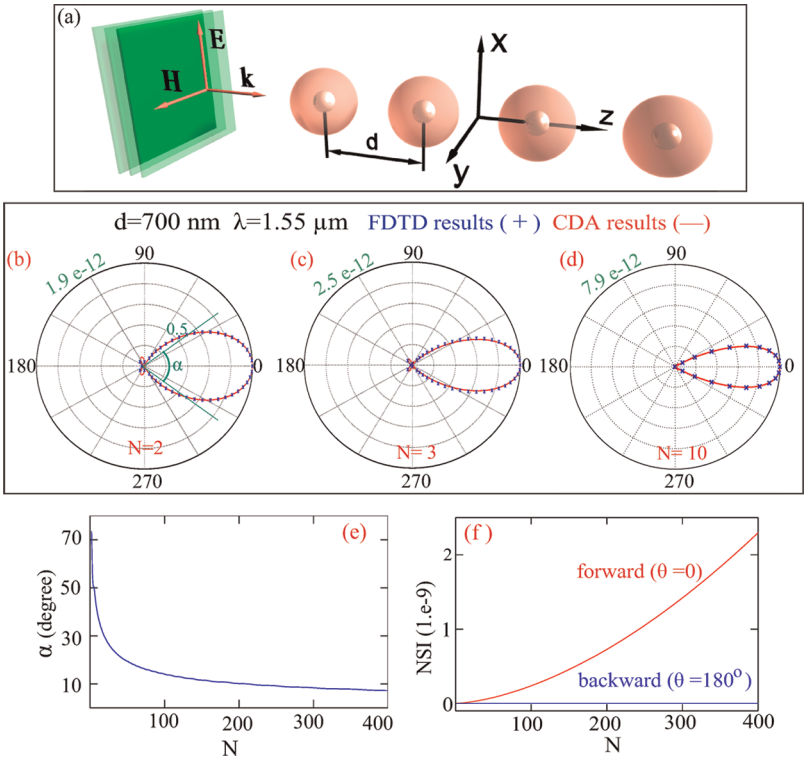

Figure 2. (a) Chain of core−shell nanoparticles with interparticle distance *d*. The chain axis is parallel to the propagation direction of the incident plane wave. (b−d) CDA (solid line) and FDTD (crosses) results of the scattering pattern (arbitrary scattering plane) by a chain of such particles with *N* = 2, 3, and 10 particles, respectively. The wavelength is λ = 1550 nm and *d* = 700 nm. The main lobe beamwidth α is defined and shown in (b). (e) Main lobe beamwidth α and (f) forward and backward normalized scattering intensity *versus* particle numbers in the chain. The parameters of a single nanoparticle are the same as in Figure 1.

is λ = 1550 nm, which is approximately the resonant wavelength of a single core−shell nanoparticle (Figure 1d), and the interparticle distance is fixed at *d* = 700 nm. It is clear from Figure 2b−d that, by increasing the number of particles, the main lobe beamwidth will decrease, indicating a better directionality. The dependence of α on the particle number is shown in Figure 2e for *N* up to 400. In Figure 2f, we also show the normalized scattering intensity in forward and backward directions for different numbers of particles in the chain. These dependencies confirm that the vanishing backward scattering feature is robust with increased particle number *N* and the forward scattering is enhanced for larger *N*. To verify the CDA results, we also perform three-dimensional finite-difference time-domain (FDTD) simulations of the chains, with the results shown in Figure 2b−d (crosses). It is seen that the FDTD results agree well with the CDA predictions, justifying the claim of azimuthally symmetric unidirectional scattering with enhanced directionality. Note here that we do not use forward−backward ratio to characterize the scattering, which is impractical in our case, as this ratio is practically infinite, as shown in Figure 2b−d. We note here that the mechanism of the directionality enhancement by the nanoparticle array is basically the same as that of Yagi-Uda antennas, where the interferences plays a major role.[16,20] However, in contrast to the conventional Yaga-Uda antennas, in our structures, the backward scattering is suppressed automatically based on the special feature of each nanoparticle, without the need of extra reflectors to reflect the backward radiation.

As a next step, we investigate the dependence of the scattering by the chain on the interparticle distance *d*. We fix *N* = 4 and λ = 1.55 μm. In Figure 3a−c, we show both the CDA (solid line) and FDTD (crosses) results of the scattering patterns for three interparticle distances: *d* = 450 nm (touching particles), 700 nm, and 1200 nm, respectively. Figure 3d shows the dependence of α on *d* for the range of 450 to 1200 nm (both FDTD and CDA results are shown). It is clear that, when *d* > 650 nm, the CDA results are in excellent agreement with the FDTD simulations, indicating the validity of the coupled dipole approximation. In the regime of *d* < 650 nm, the CDA results agree only qualitatively with the FDTD simulations, showing accurately the trend that, with decreasing *d*, α increases, displaying worse directionality. The discrepancies come from the dipole approximation of spherical particles (eq 1), which is based on the far-field scattering effect,[1,38] while the near-field features of spherical particles cannot be fully captured by the dipole approximation. Viewing the core−shell nanoparticle as combined dipoles will reflect the coupling with high accuracy when they are well separated

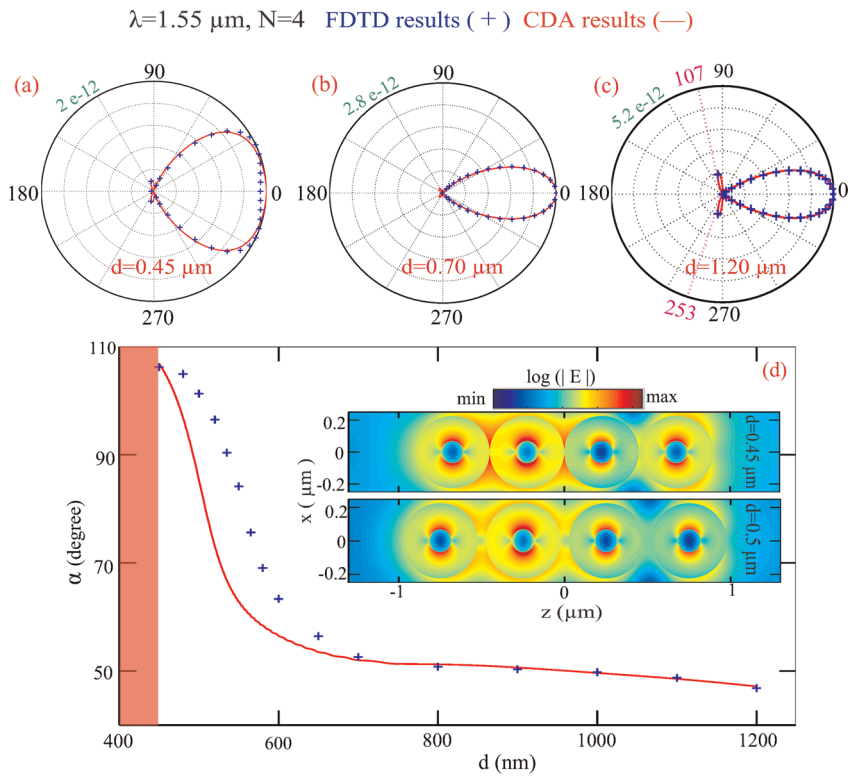

Figure 3. (a–c) CDA (solid line) and FDTD (crosses) results of the scattering pattern (arbitrary scattering plane) by a chain of core–shell nanoparticles with $N = 4$ and $d = 450$ nm (touching particles), 700 nm, and 1200 nm, respectively. Two diffraction angles of 107° and 253° are indicated in (c). (d) CDA and FDTD results of α *versus* d. Inset: Electric near-field distributions for two interparticle distances (top) $d = 450$ nm and (bottom) 500 nm. The parameters of a single particle are the same as in Figure 1d and $\lambda = 1550$ nm.

($d > 650$ nm). However, when the particles are closer to each other and the near-field coupling is more pronounced, the dipole approximation can only give qualitative trend. In Figure 3d (inset), we show the near-field distributions (electric field) for four core–shell nanoparticles of two interparticle distances, which show clearly stronger near-field coupling for smaller d. We emphasize that, even for touching particles [Figure 3d (top inset)], the dipole moments are still dominant. This is because, within each core–shell nanoparticle, the electric dipole is a result of a surface plasmon mode, with the fields confined at the interface of core and shell, while the magnetic dipole is a result of a cavity type mode in the high permittivity shell,[1,45] with most of the fields confined within the shell. Thus, the fields outside the core–shell particle are relatively small, resulting in a weak interparticle coupling. Therefore, the dipole moments remain dominant irrespective of interparticle distances [Figure 3d (inset)]. At the same time, due to the symmetry of eq 4, the dominant electric and magnetic dipole moments of each particle have the same strength, and this guarantees that the features of azimuthally symmetric scattering and vanishing backward scattering are robust against different interparticle distances (Figure 3a–d), which are preserved even for touching particles (Figure 3a).

According to Figure 3d, there is a clear trend that smaller distance d will lead to worse directionality and larger distance d can enhance the directionality. This feature can be intuitively understood simply through considering the far-field interference of the nanoparticles in the array. The phase delay between adjacent nanoparticles is $\Delta\Phi = kd(1 - \cos\theta)$, which indicates that in the forward direction $\theta = 0$ all dipoles interfere constructively. As such, the scattering intensity is always strongest in the forward direction (Figure 2b–d). At the same time, better directionality means destructive interference for smaller θ, which requires larger d to produce sufficient phase delay. Here we also emphasize the trade-off between the energy confinement and directionality for the chain with different d. Although larger d will lead to better directionality (Figure 3), when $d > \lambda/2$, the phase delay between adjacent nanoparticles will be sufficient to support collective grating diffractions, leading to significant energy leakage into other directions (Figure 3c). The angle of the first diffraction order is $\beta = \arccos(1 - \lambda/d)$, which corresponds to 107° and 253° when $d = 1200$ nm and $\lambda = 1550$ nm. As shown in Figure 3c, there is significant energy leakage into both of these directions due to the grating effect. On the other hand, for smaller d, although there will be worse directionality (Figure 3), light would be better confined (less leakage to other

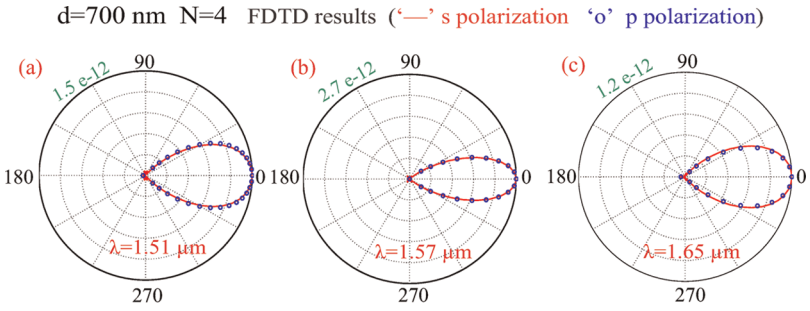

Figure 4. FDTD results of the scattering pattern of a chain of four core–shell nanoparticles with d = 700 nm for three operating wavelengths of 1.51, 1.57, and 1.65 μm. Both s (solid line) and p (circles) polarization scattering patterns are shown. The parameters of a single core–shell nanoparticle are the same as in Figure 1d.

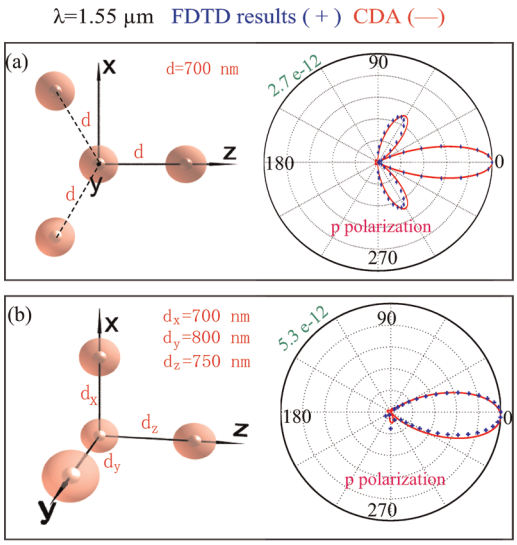

Figure 5. CDA (solid line) and FDTD (crosses) results of the p polarization scattering patterns by four core–shell nanoparticles arranged in two ways. In (a), the four particles are placed on the x–z plane occupying the three corners and the center of a equilateral triangle with nearest interparticle distance d = 700 nm, and in (b), one nanoparticle is placed at the center and other three placed at the three axes with different separations from the center. The parameters of a single core–shell nanoparticle are the same as in Figure 1.

channels) as a larger proportion of the Brillouin zone is located above the light line.[46]

A key feature of the scattering properties of the core–shell nanoparticles is their relatively broadband spectral response. From Figure 1d, one can clearly see that there is a wide spectral region where a_1 and b_1 spectrally overlap. According to eq 3, azimuthally symmetric unidirectional scattering can be achieved when a_1 and b_1 coincide and, thus, the main features should be preserved in the entire overlapping spectral region. To obtain the spectral response of the scattering, we fix the number of particles to N = 4 and the distance between them to d = 700 nm. In Figure 4a–c, we show the scattering patterns of the chain under plane wave illumination for three different wavelengths in the range of 1.51 to 1.65 μm, covering the entire C band and L band that are dominantly used in optical fiber telecommunications.[47] Both s (solid line) and p (circles) polarization scattering patterns are shown, demonstrating a 140 nm bandwidth of the unidirectional scattering. For wavelengths outside this spectral region, a_1 and b_1 are significantly different (Figure 1d), and thus both the azimuthal symmetry and the vanishing backward scattering will be lost according to eq 2. We emphasize here that we call the response broadband in a relative sense because of the following: (i) Both electric and magnetic dipolar resonances overlap spectrally over a range that is as broad as the individual resonances (Figure 1d), over which the unidirectionally scattering can be achieved. If the two resonances are not tuned to coincide spectrally and are effectively separated, the bandwidth of the unidirectional scattering will also be reduced and can be quite narrow compared to what we have achieved in this work. (ii) The achieved spectral regime covers the entire C band and L band that are primarily used in optical fiber communications.[47]

As mentioned above, in eq 4, d_i and $-m_i$, E_i and $-H_i$ are interchangeable when $\alpha_1^e = \alpha_1^m$. This means that no matter how the core–shell nanoparticles are randomly distributed, and no matter what the polarization and incident angle of the incident plane waves are, the magnetic and electric moments are of the same magnitude for each particle, thus the backward scattering is always suppressed. To verify this, in Figure 5, we show the scattering patterns for two ensemble arrangements. Four core–shell nanoparticles are arranged in two ways: (i) in the corners and the center of a equilateral triangle with nearest interparticle distance d = 700 nm (Figure 5a, left) and (ii) placed randomly in three-dimensional space (Figure 5b, left). The incident plane wave is propagating along z and polarized along x. The azimuthal symmetry of the scattering pattern is lifted since the ensemble does not possess azimuthal symmetry anymore. For simplicity in Figure 5, we only show the CDA (solid line) and FDTD (crosses) results of the scattering patterns for p polarization. It is clear that the backward scattering is vanishing for different particle distributions and should be therefore vanishing in other configurations, including the analogue of plasmonic oligomers.[42,48,49]

CONCLUSIONS

We have studied the scattering properties of (metal) core−(dielectric) shell nanoparticles and show that they exhibit azimuthally symmetric unidirectional scattering, which originates from the interference of electric and magnetic dipolar resonances that coexist with the same strength within the particle itself. We have further shown that the directionality of a single core−shell nanoparticle scattering can be enhanced when the nanoparticles are arranged in a one-dimensional chain. For such a chain, there is a trade-off between energy confinement and directionality for different interparticle distances; however, the features of vanishing backward scattering and azimuthal symmetry are always preserved irrespective of the interparticle distances, even when the particles touch each other. We also show that the operating wavelength range for unidirectional scattering of the chain spans over a bandwidth of 140 nm. Furthermore, the suppression of backward scattering, which comes from the coexistence and interference of the magnetic and electric dipoles of the core−shell nanoparticles, is a robust effect and persists for random nanoparticle distributions.

It is worth mentioning that the described features are valid under excitation of broad Gaussian beam (compared to the cross sections of the scatter),[1] which provides a feasible path to experimental observation of the predicted effects. For experimental realization, the fabrication of particles with a metal core and high-index dielectric shell is of key importance. Chemical synthesis of core−shell nanoparticles is well-suited for practical realizations,[50] with numerous examples where a metal core with a shell of high-index oxides such as TiO_2 or ZrO_2 can be routinely synthesized.[51] At the same time, for shells made of materials with a refractive index higher than 3, such as high-index semiconductors, one would probably need to resort to a bottom-up approach, including double inversion with silicon deposition. Indeed, high-index silicon shells have already been developed and used for low-Q whispering gallery mode cavities.[52] Similar shells might well be applicable for the fabrication of core−shell nanoparticles considered in this work.

We note that the operating wavelength range of the core−shell nanoparticles is highly tunable by changing the core−shell aspect ratios and the permittivity of the dielectric shell. Furthermore, there is extra freedom for resonance tuning if anisotropic materials are involved.[36,37] For the nanoparticles studied here, at the resonant wavelength of λ = 1550 nm, the total scattering efficiency is approximately 14 and the absorption efficiency is approximately 0.3. The ratio is close to 50, which means that a very small proportion of the total energy is transferred into heat rather than radiated. For an operating wavelength where the loss of metal is higher or/and the loss of the dielectric shell is significant, the absorption efficiency will be higher. Loss can also change the position and strength of the resonances of the particles. However, as long as the two resonances can be tuned to coincide spectrally with the same strength, the azimuthally symmetric unidirectional scattering could be achieved. Most importantly, all of our results can be extended to other particle geometries (rather than spheres) that support orthogonal electric and magnetic resonance pairs. We envisage that our findings on reflection suppression and broadband unidirectional scattering by superimposing electric and magnetic responses will be of great importance in various fields, especially in the flourishing fields of nanoantennas, photovoltaic devices, and nanoscale lasers that require reflection suppression.

METHODS

The plane wave (or broad Gaussian beam) scattering by spherical particles (single-layered or multilayered) can be solved analytically using Mie theory.[1,40] The far-field scattering of such particles can be expanded into orthogonal electromagnetic dipolar and multipolar scattering, with Mie coefficients a_n and b_n (both can be calculated analytically[1,40]) corresponding to electric and magnetic moments, respectively.[1,38] For the single core−shell nanoparticles investigated in this paper, the high-order scattering is effectively negligible, and the particles can be viewed as a combination of a pair of orthogonal electric and magnetic dipoles, with the effective polarizabilities calculated according to eq 1. The scattering of the core−shell nanoparticles exhibits quite unique features: vanishing backward scattering and azimuthal symmetry. All of these properties originate from the coexistence of ED and MD resonances, which coincide spectrally with the same strength. It is worth mentioning that the dipole approximation approach we used is based on the similarity of the far-field scattering pattern.[1,38] This approximation cannot be used to study the near-field properties.

In the coupled dipole approach, we employed a coupled electric and magnetic dipole approach[43,44] shown in eq 4. The resonant moments of each particle are induced not only by the fields of the incident wave but also by the scattered fields of the moments of other particles, which are considered in eq 4. By solving eq 4, electric and magnetic moments for all of the particles can be obtained, and thus the far-field scattering pattern is just a superposition of the fields of all of the dipolar moments. The specific expressions for scattered fields of both electric and magnetic moments can be found in refs 43 and 44, where a specific symmetry is shown: the electric (magnetic) field scattering matrix of an electric dipole is the same as the magnetic (electric) field scattering matrix of a magnetic dipole. This symmetry comes directly from the symmetry of Maxwell equations, and this guarantees that in eq 4 d_i and $-m_i$, E_i and $-H_i$ are exchangeable when $\alpha_1^e = \alpha_1^m$. This means that in an ensemble of randomly interacting particles with the same electric and magnetic polarizabilities, no matter how the particles are distributed, the magnetic and electric moments are of the same magnitude for each particle. This is consistent with the results shown in our paper: for a 1D chain of core−shell nanoparticles with the incident beam propagating along the chain axis, both the scattering features of azimuthal symmetry and vanishing backward scattering are preserved. As we mentioned above, the dipole approximation of each particle is based on the far-field scattering similarity. When the particles

are well separated (d > 650 nm), the coupled dipole approximation, eq 4, will give results that agree excellently with full wave 3D simulations. However, when the particles are close to each other, the dominant inducing fields are the near fields of the neighboring particles, which cannot be fully accounted for in the frame of the dipole approximation. Nevertheless, as for the core–shell nanoparticles, most of the fields are confined within the particle with only a small portion outside.[39] Therefore, even when the core–shell nanoparticles are very close together, the coupling is relatively small. As a result, the dipoles within each core–shell nanoparticle are still dominant, and the coupled dipole approximation can give qualitatively good results, even for touching particles.

All of the simulations have been carried out using the finite-difference time-domain method with the commercial software Lumerical FDTD Solutions (http://www.lumerical.com/). The experimental data[41] are assigned for the permittivity of silver, and the refractive index of the shell is n = 3.4. A total-field scattered-field plane wave source and six two-dimensional frequency-domain field monitors are used to calculate the far-field scattering pattern directly. In simulations, the perfectly matched layer (PML) boundary condition is used for all six boundaries, and we decrease the mesh size until the results are convergent.

Conflict of Interest: The authors declare no competing financial interest.

Acknowledgment. We thank A. A. Sukhorukov and I. V. Shadrivov for useful discussions, and Vincent Loke for open MATLAB codes (http://code.google.com/p/dda-si/),[53] which was extended to include both electric and magnetic responses. We acknowledge support of the Australian Research Council Centre and the National Computing Infrastructure Merit Allocation Scheme.

Note Added after ASAP Publication: After this paper was published online May 4, 2012, minor typographical changes were made for clarity. The corrected version was reposted May 15, 2012.

REFERENCES AND NOTES

1. Bohren, C. F.; Huffman, D. R. *Absorption and Scattering of Light by Small Particles*; Wiley: New York, 1983; p xiv.
2. Hirsch, L. R.; Stafford, R. J.; Bankson, J. A.; Sershen, S. R.; Rivera, B.; Price, R. E.; Hazle, J. D.; Halas, N. J.; West, J. L. Nanoshell-Mediated Near-Infrared Thermal Therapy of Tumors under Magnetic Resonance Guidance. *Proc. Natl. Acad. Sci. U.S.A.* **2003**, *100*, 13549–13554.
3. Schmid, G. *Nanoparticles: From Theory to Application*, 2nd ed.; Wiley-VCH: Weinheim, Germany, 2010; p xiii.
4. Atwater, H. A.; Polman, A. Plasmonics for Improved Photovoltaic Devices. *Nat. Mater.* **2010**, *9*, 205–213.
5. Huschka, R.; Zuloaga, J.; Knight, M. W.; Brown, L. V.; Nordlander, P.; Halas, N. J. Light-Induced Release of DNA from Gold Nanoparticles: Nanoshells and Nanorods. *J. Am. Chem. Soc.* **2011**, *133*, 12247–12255.
6. Alu, A.; Engheta, N. Cloaking a Sensor. *Phys. Rev. Lett.* **2009**, *102*, 233901.
7. Ruan, Z. C.; Fan, S. H. Superscattering of Light from Subwavelength Nanostructures. *Phys. Rev. Lett.* **2010**, *105*, 013901.
8. Verslegers, L.; Yu, Z.; Ruan, Z.; Catrysse, P. B.; Fan, S. From Electromagnetically Induced Transparency to Superscattering with a Single Structure: A Coupled-Mode Theory for Doubly Resonant Structures. *Phys. Rev. Lett.* **2012**, *108*, 083902.
9. Ni, X. J.; Emani, N. K.; Kildishev, A. V.; Boltasseva, A.; Shalaev, V. M. Broadband Light Bending with Plasmonic Nanoantennas. *Science* **2012**, *335*, 427–427.
10. Yu, N. F.; Genevet, P.; Kats, M. A.; Aieta, F.; Tetienne, J. P.; Capasso, F.; Gaburro, Z. Light Propagation with Phase Discontinuities: Generalized Laws of Reflection and Refraction. *Science* **2011**, *334*, 333–337.
11. Zhang, Y.; Grady, N. K.; Ayala-Orozco, C.; Halas, N. J. Three-Dimensional Nanostructures as Highly Efficient Generators of Second Harmonic Light. *Nano Lett.* **2011**, *11*, 5519–5523.
12. Miroshnichenko, A. E.; Luk'yanchuk, B.; Maier, S. A.; Kivshar, Y. S. Optically Induced Interaction of Magnetic Moments in Hybrid Metamaterials. *ACS Nano* **2012**, *6*, 837–842.
13. Lawandy, N. M. Localized Surface Plasmon Singularities in Amplifying Media. *Appl. Phys. Lett.* **2004**, *85*, 5040–5042.
14. Zheludev, N. I.; Prosvirnin, S. L.; Papasimakis, N.; Fedotov, V. A. Lasing Spaser. *Nat. Photonics* **2008**, *2*, 351–354.
15. Noginov, M. A.; Zhu, G.; Belgrave, A. M.; Bakker, R.; Shalaev, V. M.; Narimanov, E. E.; Stout, S.; Herz, E.; Suteewong, T.; Wiesner, U. Demonstration of a Spaser-Based Nanolase. *Nature* **2009**, *460*, 1110–1113.
16. Novotny, L.; van Hulst, N. Antennas for Light. *Nat. Photonics* **2011**, *5*, 83–90.
17. Curto, A. G.; Volpe, G.; Taminiau, T. H.; Kreuzer, M. P.; Quidant, R.; van Hulst, N. F. Unidirectional Emission of a Quantum Dot Coupled to a Nanoantenna. *Science* **2010**, *329*, 930–933.
18. Kabashin, A. V.; Evans, P.; Pastkovsky, S.; Hendren, W.; Wurtz, G. A.; Atkinson, R.; Pollard, R.; Podolskiy, V. A.; Zayats, A. V. Plasmonic Nanorod Metamaterials for Biosensing. *Nat. Mater.* **2009**, *8*, 867–871.
19. King, N. S.; Li, Y.; Ayala-Orozco, C.; Brannan, T.; Nordlander, P.; Halas, N. J. Angle- and Spectral-Dependent Light Scattering from Plasmonic Nanocups. *ACS Nano* **2011**, *5*, 7254–7262.
20. Kosako, T.; Kadoya, Y.; Hofmann, H. F. Directional Control of Light by a Nano-Optical Yagi-Uda Antenna. *Nat. Photonics* **2010**, *4*, 312–315.
21. Pakizeh, T.; Kall, M. Unidirectional Ultracompact Optical Nanoantennas. *Nano Lett.* **2009**, *9*, 2343–2349.
22. Taminiau, T. H.; Stefani, F. D.; Segerink, F. B.; Van Hulst, N. F. Optical Antennas Direct Single-Molecule Emission. *Nat. Photonics* **2008**, *2*, 234–237.
23. Evlyukhin, A. B.; Bozhevolnyi, S. I.; Pors, A.; Nielsen, M. G.; Radko, I. P.; Willatzen, M.; Albrektsen, O. Detuned Electrical Dipoles for Plasmonic Sensing. *Nano Lett.* **2010**, *10*, 4571–4577.
24. Shegai, T.; Chen, S.; Miljkovic, V. D.; Zengin, G.; Johansson, P.; Kall, M. A Bimetallic Nanoantenna for Directional Colour Routing. *Nat. Commun.* **2011**, *2*, 481.
25. Spinelli, P.; Verschuuren, M. A.; Polman, A. Broadband Omnidirectional Antireflection Coating Based on Subwavelength Surface Mie Resonators. *Nat. Commun.* **2012**, *3*, 692.
26. Shegai, T.; Miljkovic, V. D.; Bao, K.; Xu, H. X.; Nordlander, P.; Johansson, P.; Kall, M. Unidirectional Broadband Light Emission from Supported Plasmonic Nanowires. *Nano Lett.* **2011**, *11*, 706–711.
27. Miljkovic, V. D.; Shegai, T.; Kall, M.; Johansson, P. Mode-Specific Directional Emission from Hybridized Particle-on-a-Film Plasmons. *Opt. Express* **2011**, *19*, 12856–12864.
28. Li, Z. P.; Hao, F.; Huang, Y. Z.; Fang, Y. R.; Nordlander, P.; Xu, H. X. Directional Light Emission from Propagating Surface Plasmons of Silver Nanowires. *Nano Lett.* **2009**, *9*, 4383–4386.
29. Aouani, H.; Mahboub, O.; Bonod, N.; Devaux, E.; Popov, E.; Rigneault, H.; Ebbesen, T. W.; Wenger, J. Bright Unidirectional Fluorescence Emission of Molecules in a Nanoaperture with Plasmonic Corrugations. *Nano Lett.* **2011**, *11*, 637–644.
30. Rui, G. H.; Nelson, R. L.; Zhan, Q. W. Circularly Polarized Unidirectional Emission *via* a Coupled Plasmonic Spiral Antenna. *Opt. Lett.* **2011**, *36*, 4533–4535.
31. Kerker, M.; Wang, D. S.; Giles, C. L. Electromagnetic Scattering by Magnetic Spheres. *J. Opt. Soc. Am.* **1983**, *73*, 765–767.
32. Nieto-Vesperinas, M.; Saenz, J. J.; Gomez-Medina, R.; Chantada, L. Optical Forces on Small Magnetodielectric Particles. *Opt. Express* **2010**, *18*, 11428–11443.
33. Garcia-Camara, B.; Moreno, F.; Gonzalez, F.; Martin, O. J. F. Light Scattering by an Array of Electric and Magnetic Nanoparticles. *Opt. Express* **2010**, *18*, 10001–10015.
34. Gomez-Medina, R.; Garcia-Camara, B.; Suarez-Lacalle, I.; Gonzalez, F.; Moreno, F.; Nieto-Vesperinas, M.; Saenz, J. J. Electric and Magnetic Dipolar Response of Germanium Nanospheres: Interference Effects, Scattering Anisotropy, and Optical Forces. *J. Nanophotonics* **2011**, *5*, 053512.

35. Evlyukhin, A. B.; Reinhardt, C.; Seidel, A.; Luk'yanchuk, B. S.; Chichkov, B. N. Optical Response Features of Si-Nanoparticle Arrays. *Phys. Rev. B* **2010**, *82*, 043834.
36. Luk'yanchuk, B. S.; Qiu, C. W. Enhanced Scattering Efficiencies in Spherical Particles with Weakly Dissipating Anisotropic Materials. *Appl. Phys. A: Mater. Sci. Process.* **2008**, *92*, 773–776.
37. Qiu, C. W.; Luk'yanchuk, B. Peculiarities in Light Scattering by Spherical Particles with Radial Anisotropy. *J. Opt. Soc. Am. A* **2008**, *25*, 1623–1628.
38. Wheeler, M. S.; Aitchison, J. S.; Mojahedi, M. Coated Nonmagnetic Spheres with a Negative Index of Refraction at Infrared Frequencies. *Phys. Rev. B* **2006**, *73*, 045105.
39. Paniagua-Dominguez, R.; Lopez-Tejeira, F.; Marques, R.; Sanchez-Gil, J. A. Metallo-Dielectric Core−Shell Nanospheres as Building Blocks for Optical Three-Dimensional Isotropic Negative-Index Metamaterials. *New J. Phys.* **2011**, *13*, 123017.
40. Pena, O.; Pal, U. Scattering of Electromagnetic Radiation by a Multilayered Sphere. *Comput. Phys. Commun.* **2009**, *180*, 2348–2354.
41. Johnson, P. B.; Christy, R. W. Optical Constants of the Noble Metals. *Phys. Rev. B* **1972**, *6*, 4370.
42. Brandl, D. W.; Mirin, N. A.; Nordlander, P. Plasmon Modes of Nanosphere Trimers and Quadrumers. *J. Phys. Chem. B* **2006**, *110*, 12302–12310.
43. Mulholland, G. W.; Bohren, C. F.; Fuller, K. A. Light-Scattering by Agglomerates - Coupled Electric and Magnetic Dipole Method. *Langmuir* **1994**, *10*, 2533–2546.
44. Merchiers, O.; Moreno, F.; Gonzalez, F.; Saiz, J. M. Light Scattering by an Ensemble of Interacting Dipolar Particles with Both Electric and Magnetic Polarizabilities. *Phys. Rev. A* **2007**, *76*, 043834.
45. Garcia-Etxarri, A.; Gomez-Medina, R.; Froufe-Perez, L. S.; Lopez, C.; Chantada, L.; Scheffold, F.; Aizpurua, J.; Nieto-Vesperinas, M.; Saenz, J. J. Strong Magnetic Response of Submicron Silicon Particles in the Infrared. *Opt. Express* **2011**, *19*, 4815–4826.
46. Burin, A. L.; Cao, H.; Schatz, G. C.; Ratner, M. A. High-Quality Optical Modes in Low-Dimensional Arrays of Nanoparticles: Application to Random Lasers. *J. Opt. Soc. Am. B* **2004**, *21*, 121–131.
47. Ramaswami, R. Optical Fiber Communication: From Transmission to Networking. *IEEE. Commun. Mag.* **2002**, *40*, 138–147.
48. Hentschel, M.; Dregely, D.; Vogelgesang, R.; Giessen, H.; Liu, N. Plasmonic Oligomers: The Role of Individual Particles in Collective Behavior. *ACS Nano* **2011**, *5*, 2042–2050.
49. Ye, J.; Wen, F.; Sobhani, H.; Lassiter, J. B.; Dorpe, P.; Nordlander, P.; Halas, N. J. Plasmonic Nanoclusters: Near Field Properties of the Fano Resonance Interrogated with SERS. *Nano Lett.* **2012**, *12*, 1660–1667.
50. Meng, X. G.; Fujita, K.; Murai, S.; Matoba, T.; Tanaka, K. Plasmonically Controlled Lasing Resonance with Metallic-Dielectric Core−Shell Nanoparticles. *Nano Lett.* **2011**, *11*, 1374–1378.
51. Tom, R. T.; Nair, A. S.; Singh, N.; Aslam, M.; Nagendra, C. L.; Philip, R.; Vijayamohanan, K.; Pradeep, T. Freely Dispersible Au@TiO_2, Au@ZrO_2, Ag@TiO_2, and Ag@ZrO_2 Core−Shell Nanoparticles: One-Step Synthesis, Characterization, Spectroscopy, and Optical Limiting Properties. *Langmuir* **2003**, *19*, 3439–3445.
52. Yao, Y.; Yao, J.; Narasimhan, V. K.; Ruan, Z.; Xie, C.; Fan, S.; Cui, Y. Broadband Light Management Using Low-Q Whispering Gallery Modes in Spherical Nanoshells. *Nat. Commun.* **2012**, *3*, 664.
53. Loke, V. L. Y.; Menguc, M. P.; Nieminen, T. A. Discrete-Dipole Approximation with Surface Interaction: Computational Toolbox for MATLAB. *J. Quant. Spectrosc. Radiat. Transfer* **2011**, *112*, 1711–1725.